In Vivo Imaging of Human Cone Photoreceptor Inner Segments

Drew Scoles,[1] Yusufu N. Sulai,[2] Christopher S. Langlo,[3] Gerald A. Fishman,[4,5] Christine A. Curcio,[6] Joseph Carroll,[3,7–9] and Alfredo Dubra[7–9]

[1]Department of Biomedical Engineering, University of Rochester, Rochester, New York, United States
[2]The Institute of Optics, University of Rochester, Rochester, New York, United States
[3]Departments of Cell Biology, Neurobiology, and Anatomy, Medical College of Wisconsin, Milwaukee, Wisconsin, United States
[4]The Pangere Center for Inherited Retinal Diseases at the Chicago Lighthouse for People Who Are Blind or Visually Impaired, Chicago, Illinois, United States
[5]Department of Ophthalmology and Visual Sciences, University of Illinois Chicago, Chicago, Illinois, United States
[6]Department of Ophthalmology, University of Alabama at Birmingham, Birmingham, Alabama, United States
[7]Department of Ophthalmology, Medical College of Wisconsin, Milwaukee, Wisconsin, United States
[8]Department of Biophysics, Medical College of Wisconsin, Milwaukee, Wisconsin, United States
[9]Department of Biomedical Engineering, Marquette University, Milwaukee, Wisconsin, United States

Correspondence: Alfredo Dubra, Department of Ophthalmology, Medical College of Wisconsin, 925 N 87th Street, Milwaukee, WI 53226-0509, USA; adubra@mcw.edu.

DS and YNS contributed equally to the work presented here and should therefore be regarded as equivalent authors.

Submitted: April 7, 2014
Accepted: May 22, 2014

Citation: Scoles D, Sulai YN, Langlo CS, et al. In vivo imaging of human cone photoreceptor inner segments. *Invest Ophthalmol Vis Sci*. 2014;55:4244–4251. DOI:10.1167/iovs.14-14542

Purpose. An often overlooked prerequisite to cone photoreceptor gene therapy development is residual photoreceptor structure that can be rescued. While advances in adaptive optics (AO) retinal imaging have recently enabled direct visualization of individual cone and rod photoreceptors in the living human retina, these techniques largely detect strongly directionally-backscattered (waveguided) light from normal intact photoreceptors. This represents a major limitation in using existing AO imaging to quantify structure of remnant cones in degenerating retina.

Methods. Photoreceptor inner segment structure was assessed with a novel AO scanning light ophthalmoscopy (AOSLO) differential phase technique, that we termed nonconfocal split-detector, in two healthy subjects and four subjects with achromatopsia. Ex vivo preparations of five healthy donor eyes were analyzed for comparison of inner segment diameter to that measured in vivo with split-detector AOSLO.

Results. Nonconfocal split-detector AOSLO reveals the photoreceptor inner segment with or without the presence of a waveguiding outer segment. The diameter of inner segments measured in vivo is in good agreement with histology. A substantial number of foveal and parafoveal cone photoreceptors with apparently intact inner segments were identified in patients with the inherited disease achromatopsia.

Conclusions. The application of nonconfocal split-detector to emerging human gene therapy trials will improve the potential of therapeutic success, by identifying patients with sufficient retained photoreceptor structure to benefit the most from intervention. Additionally, split-detector imaging may be useful for studies of other retinal degenerations such as AMD, retinitis pigmentosa, and choroideremia where the outer segment is lost before the remainder of the photoreceptor cell.

Keywords: AOSLO, photoreceptor, gene therapy

Recently, there have been multiple successful applications of genetic[1–4] and cellular replacement[5,6] therapies to animal models of inherited blindness. Early human trials have also shown positive results,[7] demonstrating the promise of gene therapy for a wide range of human photoreceptor degenerations. These interventions aim to rescue existing dysfunctional photoreceptors using gene therapy, or restore vision by transplanting functional photoreceptors or precursor cells. A critical knowledge gap in retinal gene therapy efforts surrounds the degree of retained photoreceptor structure given a genotype and penetrance. Therefore, the lack of an objective method to directly assess the residual photoreceptor population in patients with retinal degenerations presents a roadblock for predicting the success of such therapies, especially in humans.[8]

Adaptive optics (AO) retinal imaging enables direct visualization of rod and cone structure.[9,10] Ophthalmoscopes enhanced with AO can provide images with resolution near the limit imposed by the eye's pupil diameter and axial length, by correcting for the monochromatic aberrations induced by the cornea and lens.[9] The contrast in images of the photoreceptor mosaic depends on the imaging modality and the optical properties of the photoreceptors and their surroundings. Whether imaged with an AO fundus camera, AO optical coherence tomography (AO-OCT), or a confocal AO scanning light ophthalmoscope (AOSLO), individual healthy photoreceptors appear as bright spots. This is explained by the strong

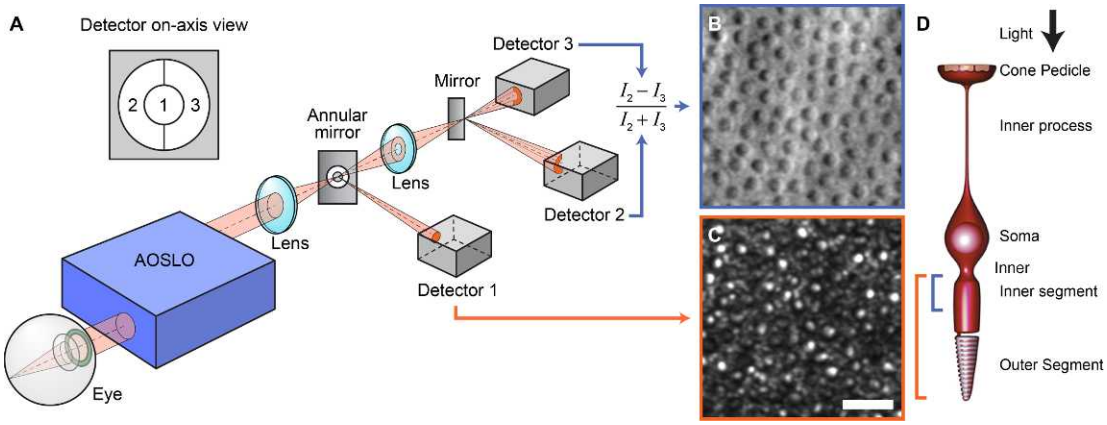

Figure 1. Schematic representations of split-detector implementation and images. (**A**) AOSLO schematic with an annular reflective mirror (*inset*) to separate the confocal from the multiple-scattered light, which is then equally divided (split) between two light detectors. The confocal signal is directly recorded in Detector 1, while the split-detector signal is the result of the subtraction of the intensities recorded in Detector 2 from Detector 3 divided by their sum at every pixel. (**B**) Representative split-detector image of the photoreceptor inner segment mosaic acquired at 10° of visual angle from fixation in a healthy volunteer, showing cones and an inability to resolve individual rods. (**C**) Simultaneously recorded confocal image showing cones with varying reflectivity surrounded by rods. *Scale bar*: 25 μm. (**D**) Photoreceptor schematic shows the likely origin of the light back reflections.

directional coupling (waveguiding) of light by the photoreceptor inner segment into the outer segment,[11] the higher refractive index relative to its surrounding and the backscattering that takes place at both ends of the photoreceptor outer segment.[12] Visualization of photoreceptors with AO ophthalmoscopy is dependent on intact outer segment morphology, and thus, the disambiguation of residual cone structure in patients with retinal degenerations remains elusive.

Here, we propose and demonstrate a nonconfocal variation of a scanning microscopy technique, known as split-detection,[13–15] to visualize the photoreceptor inner segment mosaic using an AOSLO.[16] In this method, a reflective mask with a transparent annulus is placed in the image plane where typically a circular pinhole is placed for confocal detection.[17] This mask reflects the confocal signal to a first detector and transmits the multiple-scattered light, which is then captured by two incoherent detectors that collect the light in the left and right semi-annuli (Fig. 1A). The split-detector (as we will refer to it from here on) signal is then calculated as the difference between the signals from the nonconfocal detectors, divided by their sum. In this arrangement, the waveguided light from the photoreceptor outer segment (confocal) and the multiple-scattered light from the inner segment (split-detector) can be visualized simultaneously and in perfect spatial registration (Figs. 1B, 1C). We used this imaging approach to directly examine residual cone structure in patients with achromatopsia (ACHM), revealing a robust but variable remnant cone population. Despite substantial disruption of outer retinal structure in ACHM clinical images, cone inner segment structure was observed at the foveal center in the split-detector images. The ability to directly ascertain cone structure in these patients represents an important first step toward being able to predict the therapeutic potential for gene therapy efforts on an individualized basis.

Methods

Subjects

Research procedures followed the tenets of the Declaration of Helsinki and informed written consent was obtained from all subjects after explanation of the nature and possible consequences of the study. The study protocol was approved by the institutional review board of the Medical College of Wisconsin. Patients were referred by their physicians, or self-referred for advertised studies.

Axial length measurements were obtained on all subjects (Zeiss IOL Master; Carl Zeiss Meditec, Dublin, CA, USA) in order to determine the scale (in micrometers per pixel) of each retinal image. Axial length was assumed to be constant across all eccentricities imaged in this study (0–6 mm, ~20°), as it typically varies less than 2.0% in this range.[18,19] All subjects were imaged without spectacles or trial lenses in order to avoid additional scaling errors. Prior to all retinal imaging, each eye was dilated and cycloplegia was induced through topical application of phenylephrine hydrochloride (2.5%) and tropicamide (1%).

Two visually healthy volunteers and four individuals with genetically-confirmed achromatopsia were recruited for imaging.

Genetic Testing

All four achromatopsia subjects had previously documented mutations in either *CNGA3* or *CNGB3* (see Supplementary Table S1 for a list of mutations) Testing was performed at either The John and Marcia Carver Nonprofit Genetic Testing Laboratory (University of Iowa, IA, USA) or Casey Eye Institute Molecular Diagnostics Laboratory (Oregon Health and Sciences University, OR, USA).

Optical Coherence Tomography

In all achromatopsia subjects, spectral-domain optical coherence tomography (SD-OCT) line scans were acquired (Bioptigen SD-OCT, Bioptigen, Research Triangle Park, NC, USA; or Spectralis SD-OCT, Heidelberg Engineering, Heidelberg, Germany). To improve signal to noise ratio, multiple line scans (11–22) were registered and averaged. Foveal structure was evaluated for ellipsoid zone (EZ) integrity as previously described.[20] The lateral scale of each image was estimated using the patient's axial length data.

Adaptive Optics Retinal Imaging

A custom AOSLO was modified for this study[16] to capture nonconfocal light as demonstrated by Webb et al.[21] in a split-

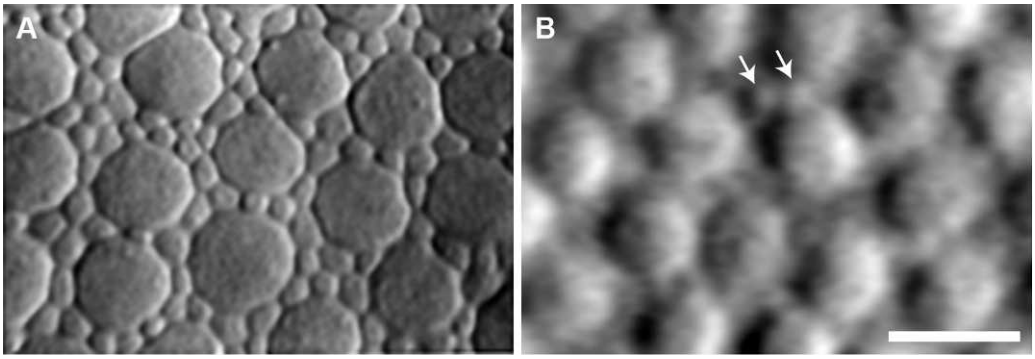

Figure 2. Side by side comparison of ex vivo[30] and in vivo imaging of the human photoreceptor inner segment mosaic at 5° temporal from fixation in different eyes. Cone inner segments are clearly resolved in (**A**) ex vivo and (**B**) in vivo, however, the resolution of the histologic images is superior due to the larger numerical aperture of the oil immersion microscope objective compared with that of the human eye (1.4 vs. 0.2). For this reason, only a few rods can be resolved in the AOSLO image (*arrows*). *Scale bar*: 10 μm.

detection configuration.[13–15] The detection path was modified by replacing the confocal aperture in the image plane in front of the detector with a reflective annular mask. The central disk of the mask was sized to reflect the central 2 Airy disk diameters (ADDs) of the focal spot toward detector 1 (confocal channel), and to transmit the remaining light up to 20 ADDs (Fig. 1). An afocal telescope relayed the plane of the mask onto a second conjugate image plane where a flat mirror with a vertical straight edge and minimal bevel divided (split) the light annulus between two additional light detectors (Fig. 1). The nonconfocal split-detection image intensity was then calculated as the difference of the detector signals divided by their sum. A multiplicative gain factor and an additive offset are used to stretch the contrast of each image for optimal display in computer monitors with 256 gray levels, while avoiding saturation. Because the light reaching the split detectors is not confocal, the detected signal cannot be interpreted through geometrical or physical optics without considering multiple scattering. Although a quantitative description of the source of contrast for this imaging method is still lacking, the resulting images resemble those that are seen in phase-gradient microscopy techniques such as differential interference contrast (DIC; Fig. 2).

The epi-illumination and the use of two detectors with on-axis point illumination as presented here is somewhat reciprocal of the oblique back-illumination method recently proposed by Ford et al.,[22] with the advantage that both symmetrically opposed detectors are recorded simultaneously, thus enabling the visualization of dynamic events such as blood flow.[23]

The imaging light source was a 790-nm super-luminescent diode (SLD; Superlum, Carrigtwohill, Co., Cork, Ireland) and the wavefront sensing light source was an 850-nm SLD (Superlum). Incident powers for these light sources were 70 and 17 μW respectively, measured at the cornea. The combined light exposure was kept 5 times below the maximum permissible exposure set forth by the ANSI Z136.1.[24,25] The output of the Hamamatsu H7422-50 photomultiplier modules (Hamamatsu Corporation, Bridgewater, NJ, USA) that were used as light detectors were amplified by a Femto HCA-10M-100K high speed current amplifier, inverted using custom electronics and digitized using a eA Helios framegrabber (Matrox Electronic Systems Ltd., Dorval, Quebec, Canada).

Image sequences were collected at the center of the fovea and from 1° to 20° visual angle lateral (temporal) to fixation using a 1.0° and 1.5° square field of view. Image sequences of 150 frames (confocal and split-detector) were collected and processed to remove the warp due to the sinusoidal motion of the horizontal scanner. Those images were then registered, and the 40 images with highest normalized cross-correlation relative to a user-selected reference frame were averaged to improve signal-to-noise ratio.[26] Because the image sequences were collected in synchrony and processed in exactly the same manner, the resulting averaged images are in perfect registration.[26]

AOSLO Image Analysis

Using the Gullstrand 2 schematic eye, the predicted 291 μm per degree of visual angle[27] was scaled linearly by the subject's axial length to determine the scale of AOSLO images. One examiner manually marked contiguous mosaics of foveal cones in split-detector AOSLO images from healthy subject AD_1225 to estimate the minimum cell size resolved with this technique. Rods were similarly marked in confocal images from AD_1225 (10° temporal) and achromat JC_10069 (parafoveal and 5° temporal) to compare rod size estimates with the resolved foveal cone size. Coordinates of marked photoreceptors were analyzed with Delaunay triangulation using custom MATLAB software (Mathworks, Natick, MA, USA) to determine the average nearest neighbor distance, which can be interpreted as an estimate of the cell size when considering a contiguous mosaic. For calculation of inner segment diameter three observers fit circles of varying diameter to best match the size of inner segments in split-detector images at multiple eccentricities in two healthy volunteers AD_1225 and AD_1207. Each observer fit 10 to 17 separate cones per image, resulting in 30 to 51 measured diameters per image.

For coarse theoretical calculation of minimum angle of resolution (MAR) in achromatopsia subjects, cone photoreceptors from the split-detector images within the central 1° of the anatomical fovea were manually marked. The average intercone distance (ICD) over a 36.5 × 36.5-μm sliding window was calculated with custom MATLAB software (Mathworks), then converted to the Nyquist cone sampling in arc minutes as described by Rossi et al.[28] The Nyquist cone sampling was assumed to be the best possible MAR, as found in the previous work in healthy subjects.[28]

Tissue Collection and Preparation

Eyes obtained from donors within 3 hours of death were preserved by immersion in 4% paraformaldehyde and 0.5% glutaraldehyde in 0.1 M PBS after the cornea and lens had been removed. Retinas were prepared as unstained whole mounts as previously described.[29] In brief, the retina was dissected free

Investigative Ophthalmology & Visual Science

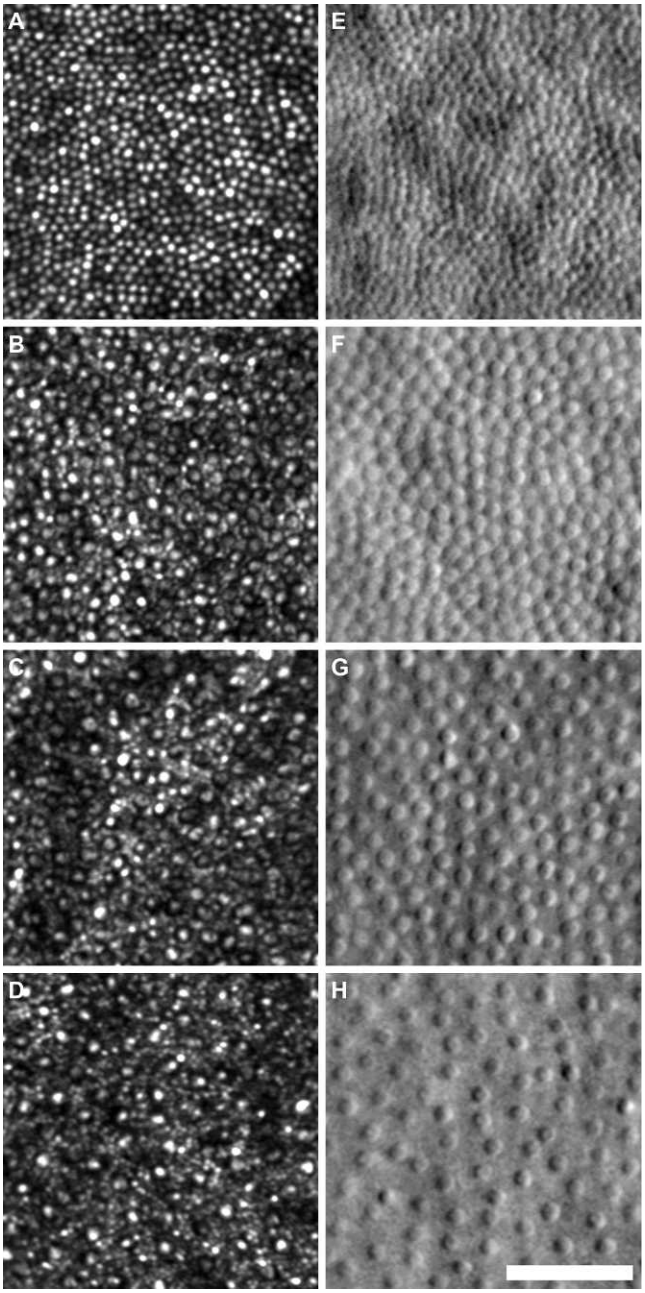

FIGURE 3. Confocal and split-detector imaging in a healthy volunteer at 1°, 5°, 10°, and 20° temporal to fixation. (**A–D**) Confocal images. (**E–H**) Split-detector images. The figure illustrates how cone photoreceptors increase in diameter with increasing eccentricity from the fovea. The increasing distance between cone inner segments is due to increasing density of rod photoreceptors, which are not resolved with split-detector imaging in most healthy volunteers. *Scale bar*: 50 μm.

from the pigment epithelium, flattened on a slide, rinsed in water, and cleared under a coverslip overnight in dimethyl sulfoxide (DMSO). Excess DMSO was blotted, 100% glycerol was applied to the tissue, and a coverslip was mounted and sealed with nail polish. A series of similarly prepared retinas underwent a slight expansion in tissue area, and inner segment diameters were not corrected for these small changes. Tissue was viewed with a combination of differential interference contrast microscopy and video (NDIC-video).

Data were obtained from five donors. Peripheral retina was analyzed in four donors, aged 27 to 35 years (H2–H5[30]). The fovea was analyzed in two donors (35-year-old male, H5[30]; 68-year-old male, eye #18[31]). The foveal centers of these eyes had an intact external limiting membrane, optically clear tissue at all levels of focus through cones, and similar peak cone density (181,800 cones/mm^2 in 35-year-old male and 170,100 cones/mm^2 in 68-year-old male).

Ex Vivo Analysis

Cone inner segment diameters in the periphery (>1 mm) of the four young retinas were determined by circle-fitting at a focusing depth where cones were optically separate. At eccentricities exceeding 1 mm, individual cone inner segments are surrounded by a ring of rods and are circular in profile. The observer centered a computer-generated circle on a NDIC-video image of a cone inner segment and adjusted its size to match the cone. Thirty cones were measured for each location, and means and SDs were computed. The mean diameter for the 30 cones obtaining by circle fitting was within 3% of the mean of the same cones as measured by outline tracing and was obtained in 40% shorter time.

Cone inner segment diameters in the foveas (<1 mm) of two eyes were calculated from component area densities (A_A) of inner segments measured with point-counting stereology[32] divided by the local density of cells, to produce an average cross-sectional area and equivalent diameter for an individual photoreceptor. The relative area of structures in a containing reference area can be estimated by counting points in a grid overlying the component and the reference area. Thus, $A_A = P_i / P_{ref}$, where P_i is the number of points overlying a specific tissue component and P_{ref} is the total number of points in the reference area, containing all components. A custom program superimposed a square grid on the NDIC-video image of the tissue, presented one grid intersection at a time for scoring, and enabled the observer to press a key indicating whether the point was over a cone, rod, or extracellular space between the inner segments. The grid used was a square lattice whose spacing between lines was determined empirically to produce relative standard errors of 5% or less for A_A of cone inner segments, the smallest of the three components over this eccentricity range, and errors of 2% to 3% for rod inner segments and extracellular space. A grid spacing of 0.0037 μm provided 100 points in a square window. A single window was scored for each location in each of two foveas, including the foveal center and at 50-μm intervals to an eccentricity of 400 μm on four cardinal meridians.

RESULTS

Split-Detector Imaging Reveals Cone Photoreceptor Inner Segment Mosaic

The photoreceptor mosaic was imaged at multiple retinal eccentricities in two subjects without known eye disease. In healthy subjects the confocal images (Figs. 3A–D), show bright spots that correspond to light waveguided by intact photoreceptors.[11] A comparison between the confocal and split-detector images reveals a 1:1 correspondence between the bright spot in the confocal image and the mound-like structures in the split-detector image (Fig. 3). The split-detector inner segment images (Figs. 1C, 3E–H) strongly resemble differential interference contrast imaging of ex vivo retinal preparations (Fig. 2). Measurements of cone structure from in vivo split-detector images in two healthy subjects showed diameters ranging from 3.0 ± 0.4 to 8.2 ± 0.6 μm (mean ±

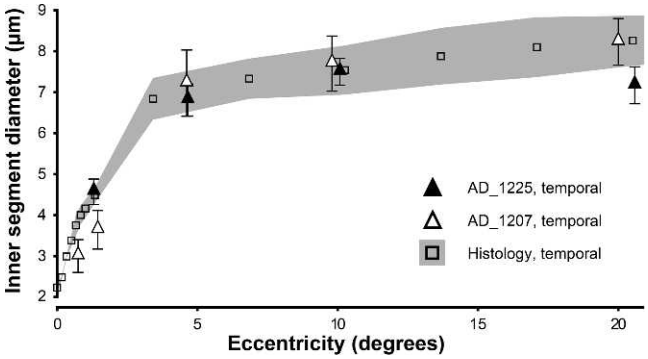

Figure 4. Plot of average cone inner segment diameter from the foveal center along temporal meridian. Ex vivo measurements are averages of two retinas (<1.4°) or four retinas (>3.4°). *Squares* indicate ex vivo measurements, and *gray shading* reflects the SD across retinas. Within 1.4° of the foveal center, measurements were averaged across all four meridians. Also shown are data from two healthy subjects measured in vivo with nonconfocal split-detection AOSLO in the temporal direction. The in vivo data is shown as *triangles* with *error bars* of ±1 SD.

SD) from 1° to 20° temporal to fixation. These measurements are consistent with ex vivo measurements at comparable retinal eccentricities, ranging from 4.2 to 8.3 μm (Fig. 4), as well as previous histologic reports in nonhuman primates.[33] The full range of ex vivo inner segment diameters measured between 0° and 41° are shown in Supplementary Table S2. Taken together, these findings support the interpretation that it is the cone inner segment, and not the outer segment, visualized by split-detector AOSLO. It is important to note that most rod and some foveal cone photoreceptors seen in the confocal images cannot be resolved in the corresponding split-detector images, suggesting a resolution limit determined either by the contrast mechanism itself or the photoreceptor refractive index profile, rather than the quality of the AO correction.

Determining the Degree of Retained Cone Photoreceptor Structure in Achromatopsia

Four patients with achromatopsia caused by mutations in the A3 or B3 subunits of cone photoreceptor cyclic nucleotide-gated (CNG) channels (Supplementary Table S1) were recruited to quantify their retained cone structure. Optical coherence tomography cross-sectional images shown in Figure 5 reveal variable central EZ disruption in all four subjects, as has been reported in many patients with achromatopsia.[20] Confocal AOSLO images in one of these subjects (JC_10069) near fixation and in the parafovea show retained waveguiding rods, with little to no reflectivity from cones (Figs. 6A, 6D) precluding identification of cone photoreceptors at these locations. The simultaneously recorded split-detector images (Figs. 6B, 6E) resolve both rod and cone inner segments. As shown best in the pseudocolor merged images (Figs. 6C, 6F), there is 1:1 correspondence between the dark circular structures in the confocal image and the mound-like structures in the split-detector image. This indicates that there can be substantial retained cone inner segment structure in patients with achromatopsia, though the altered reflectivity of the residual cones indicates morphologic disruption of the outer segments and/or disturbance of the refractive indices of the cells. In this patient, the rods are visible in the split-detector channel, unlike in healthy subjects, due to the fact that they are enlarged (see Supplementary Table S3).

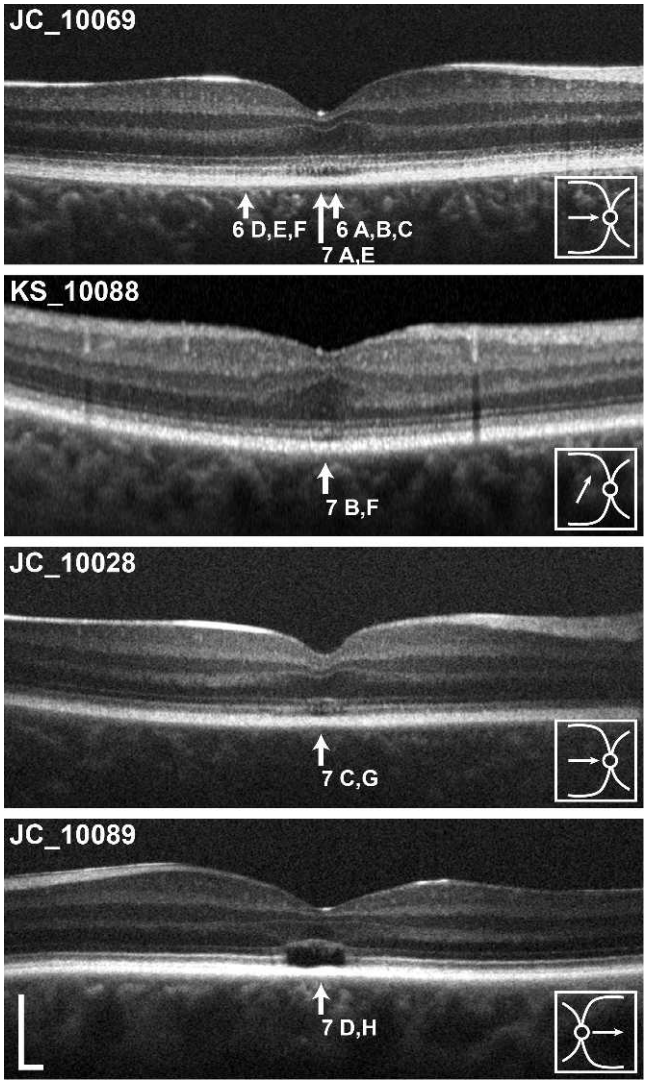

Figure 5. Spectral domain optical coherence tomography appearance of the subjects included in this study. The *top* three scans show ellipsoid zone disruption (JC_10069, KS_10088, and JC_10028), while the *bottom* shows a hyporeflective zone (JC_10089). *Arrows* indicate where AO images in corresponding figure panels were recorded. All scans show foveal hypoplasia. *Scale bar*: 200 μm.

Table. Calculation of Visual Sampling Based on Residual Cone Photoreceptor Spacing at Locations Shown in Figure 7

Subject ID #	ICD*± SD, μm	MAR†, arcmin
JC_10069	4.73 ± 0.60	0.88
KS_10088	7.59 ± 1.64	1.29
JC_10028	7.74 ± 0.95	1.52
JC_10089	14.20 ± 2.47	2.79

Assuming a best-case scenario where the entire retinal and cortical circuitry is either intact in achromatopsia or at least sufficient plasticity remains, the foveal acuity should be limited by the cone spacing. Using the calculation proposed by Rossi et al.,[29] and the measured center to center ICD over a 36.5 × 36.5-μm window from split-detector images, the achromatopsia subjects in this study show potential visual sampling that is between 1.6 and 5.3 times worse than the healthy subjects in Rossi's study.

* Cone photoreceptor center to center ICD.

† Minimum angle of resolution.

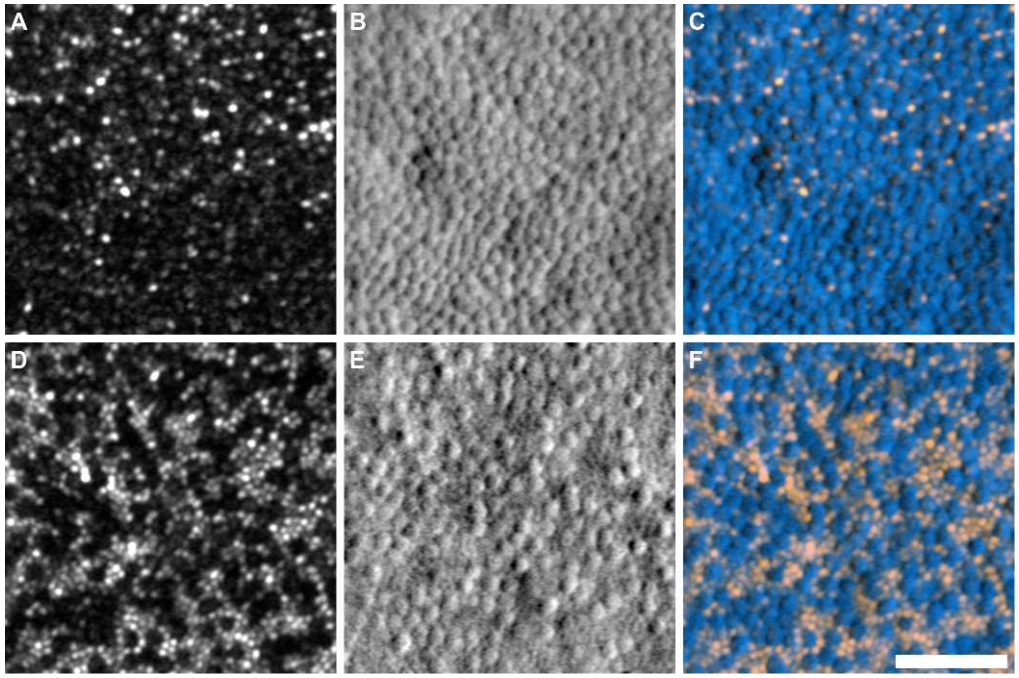

FIGURE 6. Confocal and split-detector AOSLO images of the photoreceptor mosaic in a patient with achromatopsia at 0.4° and 2° from fixation. (**A**, **D**) confocal images; (**B**, **E**) split-detector images; and (**C**, **F**) color-merged images, where the confocal image is displayed in orange, and split-detector image is shown in blue. Note the 1:1 correspondence between the dark cones in the confocal images and the inner segments in the split-detector images, highlighted by the pseudocolor images (**C**, **F**). *Scale bar*: 50 μm.

Predicted Visual Acuity

In order to estimate the best possible visual acuity recovery with gene therapy, assuming the limiting factor is photoreceptor spatial sampling, we measured the maximum cone density in four subjects with achromatopsia. Images from within 1° of the center of the anatomic fovea in all four subjects with achromatopsia are shown in Figure 7, demonstrating substantial variability in retained cone numbers across individuals. Retained cone photoreceptors were counted in these images and spatial sampling estimated based on cone spacing as previously described.[28] The spacing of retained cone photore-

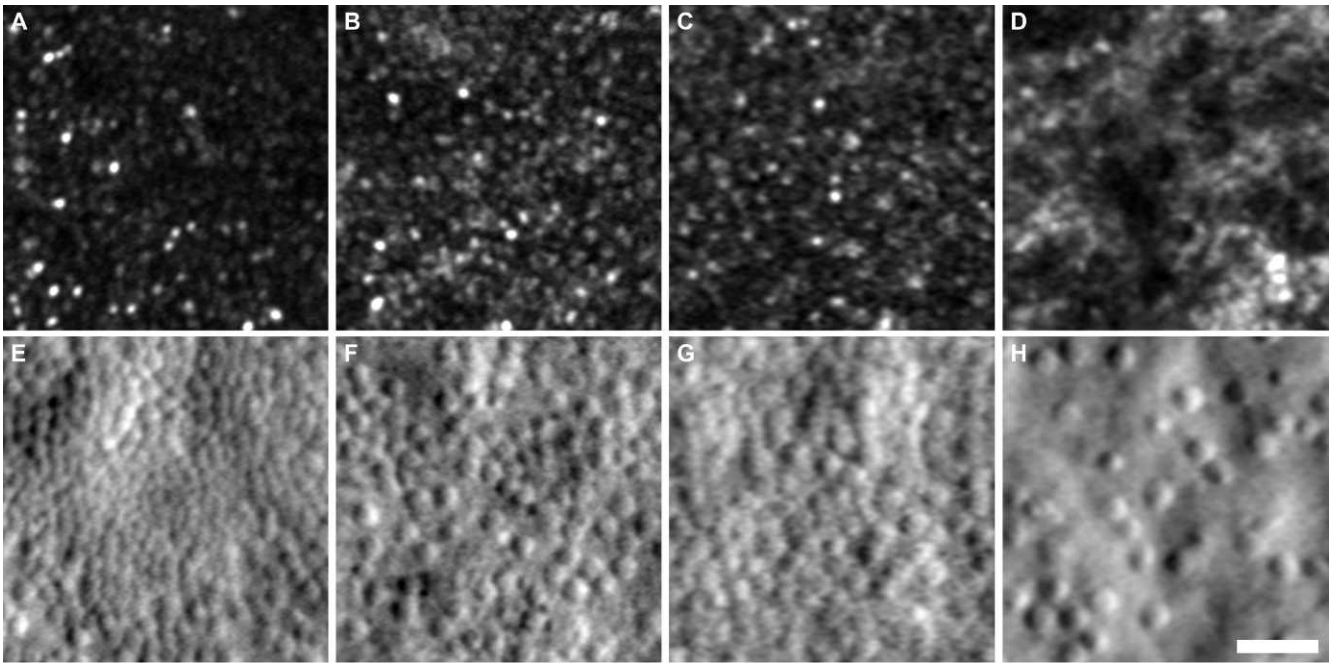

FIGURE 7. Assessing the foveal photoreceptor mosaic in achromatopsia. Confocal (*top*) and split-detector (*bottom*) AOSLO images in patient (**A**, **E**) JC_10069, (**B**, **F**) KS_10088, (**C**, **G**) JC_10028, and (**D**, **H**) JC_10089 illustrate the substantial variability of retained cone structure at the fovea between individuals and genotype. The confocal images (**A–D**) at these locations show ambiguous photoreceptor reflectivity, while the split-detector images reveal the foveal cone inner segments. *Scale bar*: 25 μm.

Investigative Ophthalmology & Visual Science

ceptors at these locations is approximately two times that of normal,[28] though it varied between the four subjects. Assuming the normal connectivity between foveal cones and midget ganglion cells is preserved,[34] this predicts an increase in minimum angle of resolution (MAR) by a factor of two to five compared with normal (Table). These results offer a promising perspective on the maximum therapeutic benefit in emerging achromatopsia gene therapy trials.

Discussion

Split-detector imaging provides a robust method to visualize cone inner segment structure in a manner that appears to be independent of the integrity of the outer segment. Conventional AO (confocal, flood-illuminated, and OCT) imaging relies on a waveguided reflection from an intact, correctly oriented outer segment to visualize cones.[11] However, outer segment structure degenerates in a variety of retinal diseases, including retinitis pigmentosa,[35–37] AMD,[38,39] and choroideremia.[40] Quantification of cone structure in AO retinal images had until now been based on detecting visible waveguiding cones, with dark areas in the mosaic often interpreted as devoid of photoreceptors. Using the split-detector technique in patients with achromatopsia, we showed that cone inner segments occupied the majority of the dark gaps in the confocal AOSLO photoreceptor images. This provides the first direct in vivo evidence of substantial remnant cone structure in patients with achromatopsia, and demonstrates that analyses based only on confocal/bright field signals will underestimate the degree of residual cone structure. A similar "dark cone" appearance has been described in a number of other conditions,[41–44] suggesting that split-detector AOSLO imaging would provide a more direct quantification of cone structure in these patients as well.

Previous studies of achromatopsia have measured the reflectivity of the EZ and the thickness of the outer nuclear layer (ONL) with OCT[20,45,46] to assess the remaining cone photoreceptor population. Neither of these analyses can distinguish between contributions of rods and cones, due to insufficient transverse image resolution. More recently, parafoveal cone structure has been estimated with AOSLO in achromatopsia[47] and blue-cone monochromacy[48] by using rings of rods to facilitate counting of presumed nonwaveguiding cones. However, this is not possible at the foveola where a there is a contiguous dark patch without rods, and in other conditions in which rods also degenerate (such as retinitis pigmentosa), the ability to use intact rods to infer the presence of a perifoveal cone is limited. Moreover, in other retinal degenerations, the RPE can sometimes be resolved[49] and often contains structures with reflectance profiles similar to small photoreceptors. Disambiguating RPE from photoreceptor structure in these cases is difficult, if not impossible, using only confocal AOSLO imaging. Split-detector imaging should be invaluable in elucidating cone structure in these more complex retinal diseases.

The direct visualization of cone structure in achromatopsia afforded through the use of split-detector AOSLO stands to benefit emerging gene therapy efforts. Prior to intervention these images could be used to predict the anatomic upper limit of visual recovery that may change with genotype and age.[46] In addition, knowledge of the degree of residual foveal cone structure could inform the estimation of the relative risk to benefit ratio on an individualized basis, and one could actually select patients for inclusion based on the amount of remnant cone structure. Beyond achromatopsia, the new split-detector AOSLO technique could positively impact the design and recruitment for clinical trials for other retinal degenerations involving damage to the photoreceptor outer segment.

Acknowledgments

The entire imaging and hardware control software were developed by Zachary G. Harvey. ZGH also made substantial contributions to the adaptive optics control and image registration software. The authors thank Carol White, Fred Collison, Robert F. Cooper, and Kimberly E. Stepien in the preparation of this manuscript.

Supported by the National Institutes of Health (NIH; Bethesda, MD, USA) Grants P30EY001931, R01EY017607, R01EY006109, UL1TR000055, T32GM007356, and T32GM080202. A Career Development Award from Research to Prevent Blindness (New York, NY, USA) and a Career Award at the Scientific Interface from the Burroughs Wellcome Fund (ADS; Durham, NC, USA). Institutional support from EyeSight Foundation of Alabama (CC; Birmingham, AL, USA). This research was also supported by grants from the RD & Linda Peters Foundation (Brillion, WI, USA), Gene & Ruth Posner Foundation (Milwaukee, WI, USA), Foundation Fighting Blindness (Columbia, MD, USA), and unrestricted departmental grants from Research to Prevent Blindness and the Glaucoma Research Foundation Catalyst for a Cure Initiative (San Francisco, CA, USA). This investigation was conducted in a facility constructed with support from the Research Facilities Improvement Program; grant number C06-RR016511 from the National Center for Research Resources, NIH.

Disclosure: **D. Scoles**, None; **Y.N. Sulai**, None; **C.S. Langlo**, None; **G.A. Fishman**, None; **C.A. Curcio**, None; **J. Carroll**, None; **A. Dubra**, Canon USA, Inc. (C)

References

1. Alexander JJ, Umino Y, Everhart D, et al. Restoration of cone vision in a mouse model of achromatopsia. *Nat Med*. 2007;13:685–687.
2. Pang JJ, Deng WT, Dai X, et al. AAV-mediated cone rescue in a naturally occurring mouse model of CNGA3-achromatopsia. *PLoS One*. 2012;7:e35250.
3. Mancuso K, Hauswirth WW, Li Q, et al. Gene therapy for red-green colour blindness in adult primates. *Nature*. 2009;461:784–787.
4. Komaromy AM, Alexander JJ, Rowlan JS, et al. Gene therapy rescues cone function in congenital achromatopsia. *Hum Mol Genet*. 2010;19:2581–2593.
5. Pearson RA, Barber AC, Rizzi M, et al. Restoration of vision after transplantation of photoreceptors. *Nature*. 2012;485:99–103.
6. MacLaren RE, Pearson RA, MacNeil A, et al. Retinal repair by transplantation of photoreceptor precursors. *Nature*. 2006;444:203–207.
7. Maclaren RE, Groppe M, Barnard AR, et al. Retinal gene therapy in patients with choroideremia: initial findings from a phase 1/2 clinical trial. *Lancet*. 2014;383:1129–1137.
8. Jacobson SG, Aleman TS, Cideciyan AV, et al. Identifying photoreceptors in blind eyes caused by RPE65 mutations: prerequisite for human gene therapy success. *Proc Natl Acad Sci U S A*. 2005;102:6177–6182.
9. Liang J, Williams DR. Aberrations and retinal image quality of the normal human eye. *J Opt Soc Am A*. 1997;14:2873–2883.
10. Dubra A, Sulai Y, Norris JL, et al. Noninvasive imaging of the human rod photoreceptor mosaic using a confocal adaptive optics scanning ophthalmoscope. *Biomed Opt Express*. 2011;2:1864–1876.
11. Miller DT, Williams DR, Morris GM, Liang J. Images of cone photoreceptors in the living human eye. *Vision Res*. 1996;36:1067–1079.
12. Kocaoglu OP, Lee S, Jonnal RS, et al. Imaging cone photoreceptors in three dimensions and in time using ultrahigh resolution optical coherence tomography with adaptive optics. *Biomed Opt Express*. 2011;2:748–763.

13. Hamilton DK, Sheppard CJR. Differential phase-contrast in scanning optical microscopy. *J Microsc*. 1984;133:27–39.
14. Wilson T, Hamilton D. Differential amplitude contrast imaging in the scanning optical microscope. *Appl Phys B*. 1983;32: 187–191.
15. Amos WB, Reichelt S, Cattermole DM, Laufer J. Re-evaluation of differential phase contrast (DPC) in a scanning laser microscope using a split detector as an alternative to differential interference contrast (DIC) optics. *J Microsc*. 2003;210:166–175.
16. Dubra A, Sulai Y. Reflective afocal broadband adaptive optics scanning ophthalmoscope. *Biomed Opt Express*. 2011;2: 1757–1768.
17. Roorda A, Romero-Borja F, Donnelly WJ, Queener H, Hebert TJ, Campbell MCW. Adaptive optics scanning laser ophthalmoscopy. *Opt Express*. 2002;10:405–412.
18. Calver R, Radhakrishnan H, Osuobeni E, O'Leary D. Peripheral refraction for distance and near vision in emmetropes and myopes. *Ophthalmic Physiol Opt*. 2007;27:584–593.
19. Mallen EAH, Kashyap P. Technical note: measurement of retinal contour and supine axial length using the Zeiss IOLMaster. *Ophthalmic Physiol Opt*. 2007;27:404–411.
20. Sundaram V, Wilde C, Aboshiha J, et al. Retinal structure and function in achromatopsia: implications for gene therapy. *Ophthalmology*. 2014;121:234–245.
21. Webb RH, Hughes GW, Delori FC. Confocal scanning laser ophthalmoscope. *Appl Optics*. 1987;26:1492–1499.
22. Ford TN, Chu KK, Mertz J. Phase-gradient microscopy in thick tissue with oblique back-illumination. *Nat Methods*. 2012;9: 1195–1197.
23. Sulai YN, Scoles D, Harvey Z, Dubra A. Visualization of retinal vascular structure and perfusion with a nonconfocal adaptive optics scanning light ophthalmoscope. *J Opt Soc Am A*. 2014; 31:569–579.
24. ANSI. *American National Standard for Safe Use of Lasers in Research, Development, or Testing*. Orlando, FL: Laser Institute of America; 2007.
25. Delori FC, Webb RH, Sliney DH. Maximum permissible exposures for ocular safety (ANSI 2000), with emphasis on ophthalmic devices. *J Opt Soc Am A*. 2007;24:1250–1265.
26. Dubra A, Harvey Z. *Registration of 2D Images from Fast Scanning Ophthalmic Instruments. The 4th International Workshop on Biomedical Image Registration*. Lübeck: Springer-Verlag; 2010.
27. Hirsch J, Curcio CA. The spatial resolution capacity of human foveal retina. *Vision Res*. 1989;29:1095–1101.
28. Rossi EA, Roorda A. The relationship between visual resolution and cone spacing in the human fovea. *Nat Neurosci*. 2010;13:156–157.
29. Curcio CA, Packer O, Kalina RE. A whole mount method for sequential analysis of photoreceptor and ganglion cell topography in a single retina. *Vision Res*. 1987;27:9–15.
30. Curcio CA, Sloan KR, Kalina RE, Hendrickson AE. Human photoreceptor topography. *J Comp Neurol*. 1990;292:497–523.
31. Curcio CA, Millican CL, Allen KA, Kalina RE. Aging of the human photoreceptor mosaic: evidence for selective vulnerability of rods in central retina. *Invest Ophthalmol Vis Sci*. 1993;34:3278–3296.
32. Weibel ER. *Stereological Methods*. New York: Academic Press; 1979.
33. Packer O, Hendrickson AE, Curcio CA. Photoreceptor topography of the retina in the adult pigtail macaque (*Macaca nemestrina*). *J Comp Neurol*. 1989;288:165–183.
34. Drasdo N, Millican CL, Katholi CR, Curcio CA. The length of Henle fibers in the human retina and a model of ganglion receptive field density in the visual field. *Vision Res*. 2007;47: 2901–2911.
35. Kolb H, Gouras P. Electron microscopic observations of human retinitis pigmentosa, dominantly inherited. *Invest Ophthalmol*. 1974;13:487–498.
36. Szamier RB, Berson EL. Retinal ultrastructure in advanced retinitis pigmentosa. *Invest Ophthalmol Vis Sci*. 1977;16:947–962.
37. Gao J, Cheon K, Nusinowitz S, et al. Progressive photoreceptor degeneration, outer segment dysplasia, and rhodopsin mislocalization in mice with targeted disruption of the retinitis pigmentosa-1 (Rp1) gene. *Proc Natl Acad Sci U S A*. 2002;99: 5698–5703.
38. Johnson PT, Lewis GP, Talaga KC, et al. Drusen-associated degeneration in the retina. *Invest Ophthalmol Vis Sci*. 2003; 44:4481–4488.
39. Curcio CA, Medeiros NE, Millican CL. Photoreceptor loss in age-related macular degeneration. *Invest Ophthalmol Vis Sci*. 1996;37:1236–1249.
40. Syed N, Smith JE, John SK, Seabra MC, Aguirre GD, Milam AH. Evaluation of retinal photoreceptors and pigment epithelium in a female carrier of choroideremia. *Ophthalmology*. 2001; 108:711–720.
41. Joeres S, Jones SM, Chen DC, et al. Retinal imaging with adaptive optics scanning laser ophthalmoscopy in unexplained central ring scotoma. *Arch Ophthalmol*. 2008;126: 543–547.
42. Carroll J, Kay DB, Scoles D, Dubra A, Lombardo M. Adaptive optics retinal imaging–clinical opportunities and challenges. *Curr Eye Res*. 2013;38:709–721.
43. Makiyama Y, Ooto S, Hangai M, et al. Macular cone abnormalities in retinitis pigmentosa with preserved central vision using adaptive optics scanning laser ophthalmoscopy. *PLoS One*. 2013;8:e79447.
44. Yokota S, Ooto S, Hangai M, et al. Objective assessment of foveal cone loss ratio in surgically closed macular holes using adaptive optics scanning laser ophthalmoscopy. *PLoS One*. 2013;8:e63786.
45. Hood DC, Zhang X, Ramachandran R, et al. The inner segment/outer segment border seen on optical coherence tomography is less intense in patients with diminished cone function. *Invest Ophthalmol Vis Sci*. 2011;52:9703–9709.
46. Thomas MG, McLean RJ, Kohl S, Sheth V, Gottlob I. Early signs of longitudinal progressive cone photoreceptor degeneration in achromatopsia. *Br J Ophthalmol*. 2012;96:1232–1236.
47. Genead MA, Fishman GA, Rha J, et al. Photoreceptor structure and function in patients with congenital achromatopsia. *Invest Ophthalmol Vis Sci*. 2011;52:7298–7308.
48. Cideciyan AV, Hufnagel RB, Carroll J, et al. Human cone visual pigment deletions spare sufficient photoreceptors to warrant gene therapy. *Hum Gene Ther*. 2013;24:993–1006.
49. Roorda A, Zhang Y, Duncan JL. High-resolution in vivo imaging of the RPE mosaic in eyes with retinal disease. *Invest Ophthalmol Vis Sci*. 2007;48:2297–2303.

Investigative Ophthalmology & Visual Science